Inherent Strain and Its Application for Prediction of Welding Deformation at Groove in Narrow Gap Welding†

Hidekazu MURAKAWA*, Yu LUO and Takeshi KOIDE*****

Abstract

Welding deformation and welding residual stress are produced by the inherent strain which is created during the thermal cycle. If the inherent strain is known, both deformation and residual stress can be computed by simple elastic analysis. The magnitude and the distribution of the inherent strain depend mainly on highest temperature reached and the constraint. In case of narrow gap welding, the deformation at the groove is strongly influenced by constraint in various forms. Thus, the characteristics of the inherent strain in narrow gap welding are clarified from the aspect of constraint using the thermal-elastic-plastic FEM analysis in this report. Further, formulas to describe the inherent strain are proposed and apply them to the prediction welding deformations.

KEY WORDS: (Welding Deformation) (Narrow Gap Welding) (Multi-Pass Welding) (Inherent Strain) (Theoretical Prediction) (Constraint)

1. Introduction

The narrow gap welding is an efficient welding method for the welding of thick sections. However, depending on the geometry of the structure and the external constraint, the shrinkage of the groove gap during the multi-pass welding may exceeds the limit to obtain sound weld. To prevent this type of problem, theoretical prediction is effective. The welding residual stresses and distortions are produced by inherent strain[1-3]. If the inherent strain is known for the welding joint with given geometry and welding conditions, the welding deformation can be computed by simple elastic finite element analysis. In this report, the characteristics of the inherent strain in the narrow gap welding are clarified using thermal-elastic-plastic FEM analysis. Based on the computed results, formulas to describe the inherent strain are proposed and their validity is demonstrated through comparison with experiments.

2. Concept of Inherent Strain

In general, mechanical behavior of elastic plastic material under a thermal cycle can be described by,

(1) strain-displacement relation

(2) stress-strain relation

(3) equilibrium condition

(4) proper boundary conditions

Among these, stress-strain relation is the most important in the welding mechanics. One of the fundamental assumptions is that the total strain can be separated into the sum of the strain components produced by different processes, i.e.,

$$\varepsilon = \varepsilon^e + \varepsilon^p + \varepsilon^t \quad (1)$$

Where, ε, ε^e, ε^p and ε^t are the total, the elastic, the plastic and the thermal strain, respectively. Since, the thermal strain disappears when the temperature returns to the room temperature after the thermal cycle, Eq. 1 becomes,

$$\varepsilon = \varepsilon^e + \varepsilon^p \quad (2)$$

Where the elastic strain ε^e is produced by the residual stress and the total strain ε corresponds to the residual deformation. By rewriting Eq. 2 as,

$$\varepsilon^*(\text{inherent strain}) = \varepsilon^p = \varepsilon\ (\text{residual deformation}) - \varepsilon^e(\text{residual stress}) \quad (3)$$

it is seen, conceptually, that the residual stress and the residual deformation are produced by the inherent strain. In other words, the residual stress and the residual

† Received on June 1, 1998

* Associate Professor
** Contract Reseracher, IEM
*** Graduate Student

Transactions of JWRI is published by Joining and Welding Research Institute of Osaka University, Ibaraki, Osaka 567-0047, Japan.

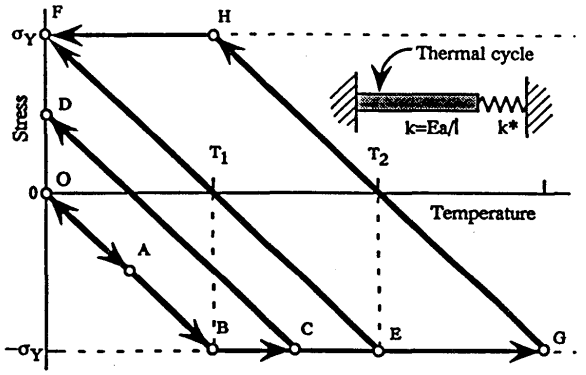

Fig. 1 Stress history of bar with elastic constraint under thermal cycle.

deformation can be estimated when the inherent strain is known. In case of the thermal-elastic-plastic problem, the inherent strain is the residual plastic strain itself if there is no initial stress or initial gap in geometry. When the problem involves phenomena, such as creep and phase transformation, creep strain and volumetric change due to the transformation can be included in Eqs. 1 and 3 as a part of the inelastic strain and the inherent strain.

The mechanism in which the inherent strain is produced during thermal cycle can be explained by using a simple model of a metal bar constrained by an elastic spring[4] as shown in **Fig. 1**. When the bar is heated to T_{max} from the room temperature (zero degree) and cooled down to the room temperature, the compressive thermal stress is produced in the heating process as shown in the figure. The phenomena change with the value of the maximum temperature T_{max} relative to T_1 and T_2, which are defined as,

$$T_1=\sigma_Y/\beta\alpha E \quad (4)$$

$$T_2= 2T_1$$

where, E: Young's modulus
σ_Y: yield stress
α: thermal expansion ratio
β: constraint parameter defined using the stiffness of the bar k and the spring k* as in the following equations.

$$\beta=k^*/(k+k^*) \quad (5)$$

k=aE/L stiffness of bar
k* stiffness of spring
a cross-sectional area of bar
L length of bar

When $T_{max}<T_1$, the thermal stress does not reach the compressive yield stress in the heating process. Thus, no plastic strain (inherent strain : ε^*) is produced. Since there is no inherent strain, no residual stress nor residual deformation is produced.

When $T_1<T_{max}<T_2$, the thermal stress reaches the yield stress and compressive inherent strain is produced. However, the behavior of the bar is elastic in the cooling process. The inherent strain ε^*, residual stress σ_R and the residual deformation δ_R in this case are,

$$\varepsilon^* = -T_{max}\,\alpha + \varepsilon_Y/\beta = -T_{max}\,\alpha + \sigma_Y/E\beta \quad (6)$$

$$\sigma_R = -\beta E\,\varepsilon^* = \beta\,T_{max}\,\alpha\,E - \sigma_Y$$

$$\delta_R = (\varepsilon^* + \varepsilon^e)L = (1-\beta)(-T_{max}\,\alpha + \sigma_Y/E\beta)L$$

When $T_{max}>T_2$, plastic deformation takes place in both the heating and the cooling processes. The residual stress σ_R and the residual deformation δ_R are

$$\varepsilon^* = -\varepsilon_Y/\beta = -\sigma_Y/E\beta \quad (7)$$

$$\sigma_R = \sigma_Y$$

$$\delta_R = (\varepsilon^* + \varepsilon^e)L = (1-1/\beta)\,\varepsilon_Y\,L$$

As it is seen from Eqs. 6 and 7, the inherent strain is strongly influenced by both the highest temperature T_{max} and the constraint parameter β.

3. Effect of Constraint

Figure 2 shows two models of narrow gap welding to clarify the effect of constraint on the deformation at the groove. The models (a) and (b) are designed to have small and large constraint, respectively. The thickness of the plate is 200 mm. The welding is done by high

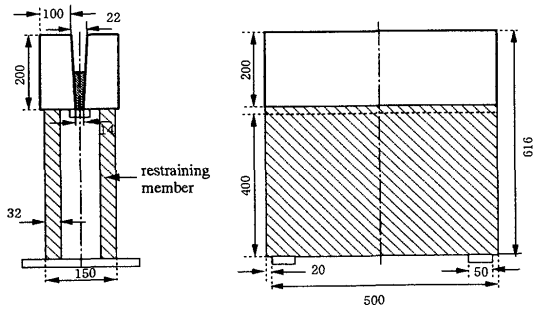

(a) model with small constraint

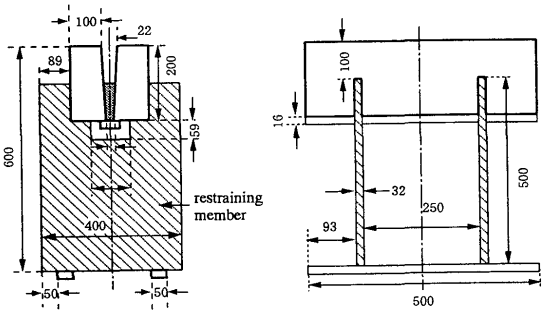

(b) model with large constraint

Fig. 2 Models of narrow gap welding.

Table1 Welding condition for narrow gap welding in experiment.

Material	Wire	Current (A)	Voltage (V)	Welding speed (cm/min)	Rotating speed (Hz)	Preheating and Interpass temperature (℃)
SS400	YM-2 (1.2mm)	350	35	25	50	100

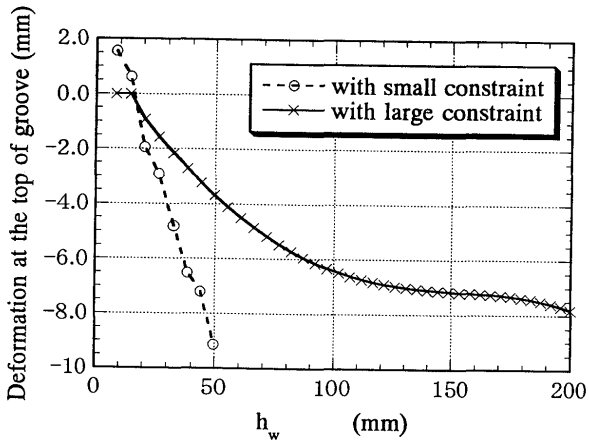

Fig. 3 Measured change of groove gap with number of welding paths.

speed rotating arc narrow gap welding. The total welding paths is 40 and the welding condition is given in **Table 1**. The deformation at the top of the groove measured for the two models are plotted against the throat thickness or the thickness of the weld finished up to the current stage h_W in **Fig. 3**. As it is seen from the figure, the groove is closed very quickly when the constraint is small. Due to the excessive closure of the groove, the welding becomes practically impossible after 8 paths in case of the model with small constraint.

The deformation of these two models are analyzed as plane strain problem using ABAQUS. **Figure 4** shows the assumed temperature dependent material properties employed in the analyses. The mesh division is shown in **Fig. 5.** The computed deformations are compared with experiments in **Fig. 6.** It is noticed that the computed deformations are too small compared to the measured ones in the early stage of the welding. However, the curves for experiment with large constraint and two computations for cases with small and large constraints become almost parallel to each other in the latter half of the welding process. This phenomenon can be explained from the aspect of constraint. The constraint can be separated into external and internal constraints. Further, internal constraint can be divided into in-plane constraint and the constraint due to the effect of moving heat source. The former is acting in the plane normal to the welding direction. This type of constraint is considered in the two-dimensional analysis assuming the plane strain state. The latter is the constraint, which comes from the variation of the

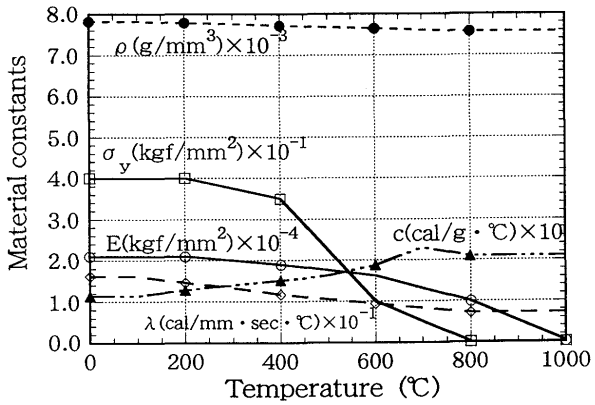

Fig. 4 Temperature dependence of material constants assumed in analysis.

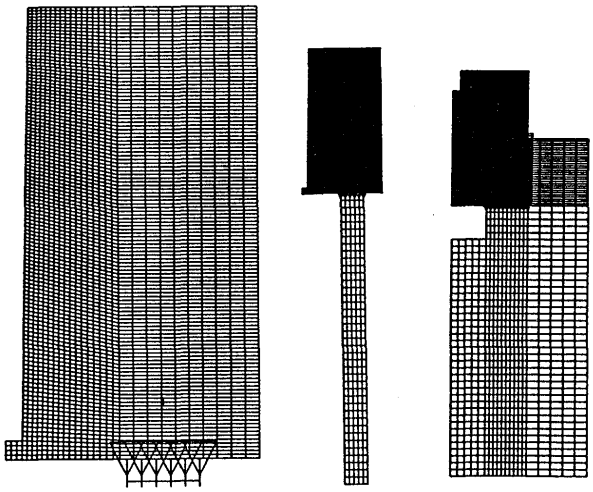

Fig. 5 Finite element mesh division.

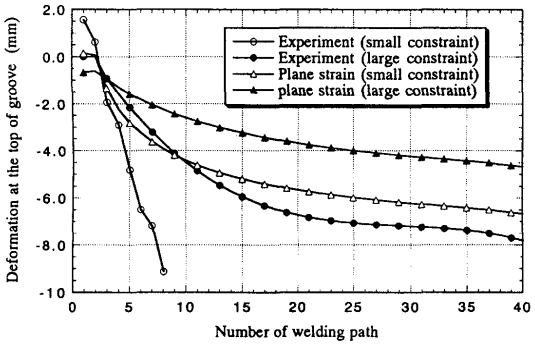

Fig. 6 Comparison between experiments and computations.

mechanical state along the welding direction. This type of constraint can not be considered in plane strain model. Among these three types of constraint, only in-plane constraint increases with the number of welding paths while external constraint and the effect of moving heat source remain unchanged. Noting that in-plane part of internal constraint becomes dominant in the last half stage of the welding, it is explained that the characteristics of deformation in experiment with large constraint and two computed results are almost identical. This implies that the effect of external constraint and that

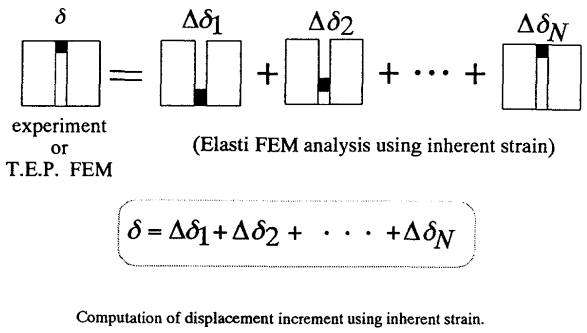

Fig. 7 Procedure of elastic analysis using inherent strain.

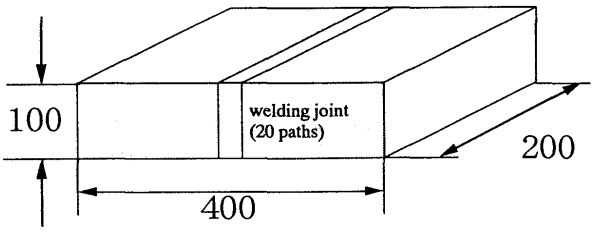

Fig. 8 Multi-pass welding model without external constraint.

of moving heat source have significance influence only in the early stage of the multi pass welding. For the analysis of this stage, three-dimensional model in which both external constraint and the effect of moving heat source are considered must be employed. However if enough number of welding paths are laid so that the inplane constraint becomes dominant, plane strain model can be used.

4. Prediction of Deformation by Elastic FEM

Since the welding deformation and the residual stress are produced by inherent strain, the deformation of the groove during multi-pass welding can be computed through a serial elastic computations using inherent strain as illustrated by **Fig. 7.** The deformation after N-th path can be computed as the sum of the deformation increment $\Delta\delta_i$ from the first path to the N-th path. The deformation increment $\Delta\delta_i$ is computed by applying known inherent strain to the area of weld metal.

5. Estimation of Inherent Strain

In general the inherent strain has six components and each component has rather complex distribution. If our porpoise is limited to predict the deformation at groove, it is a reasonable approximation that only the transverse component of the inherent strain is considered and it

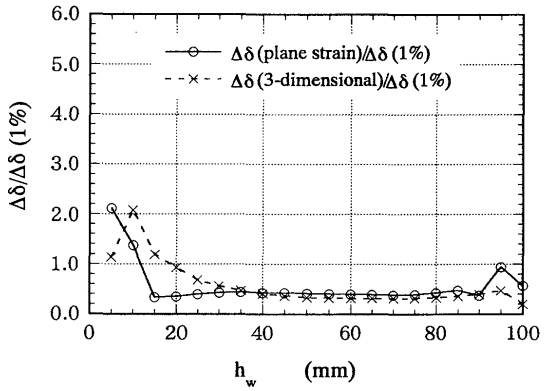

Fig. 9 Inherent strains estimated from 3-D and plane strain thermal-elastic-plastic analyses.

distributes uniformly in the cross-section of each welding path. Based on this assumption, the magnitude of inherent strain at each welding path can be estimated from experimental measurement or FEM analysis in the following manner. Let's take the plate without external constraint shown in **Fig. 8** as an example. Assuming that reliable computed result is available, perform elastic computations for each welding path. In these elastic computations, the groove is filled with metal up to the i-th path to be considered. The inherent strain with its magnitude of 1 % is introduced to the elements for the i-th path and the deformation at the top of the groove due to this inherent strain is computed. The computed deformation $\Delta\delta(1\%)$ corresponds to the change or the increment of deformation at groove due to the welding of the i-th path. Thus the magnitude of the inherent strain for the i-th path ε^*_i is determined by the following equation.

$$\varepsilon^*_i = 0.01\Delta\delta/\Delta\delta(1\%) \quad (8)$$

where $\Delta\delta$ is the increment of the deformation at groove computed by thermal-elastic-plastic FEM.

Figure 9 shows the ratio $\Delta\delta/\Delta\delta(1\%)$ for the plate without external constraint computed using three-dimensional FEM and plane strain FEM models. In general, the magnitude of inherent strain is mainly governed by maximum temperature Tmax and local constraint. From the aspect of temperature, local temperature distribution near i-th path is almost the same for all paths except for the first and the last few paths for which the surface effect appears. Noting this, significant difference between three-dimensional model and plane strain model is observed only welding up to h_w=30 mm. After 30 mm, the value of $\Delta\delta/\Delta\delta(1\%)$, or the inherent strain ε^*_i , is almost constant and its value for three-dimensional model and plane strain model is almost the same. This implies that the local constraints in the two models become same after the thickness of

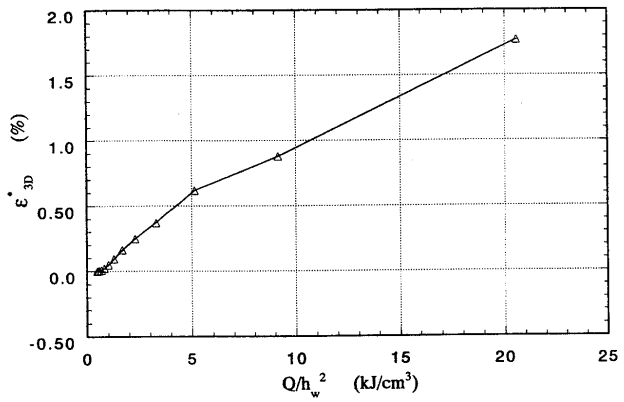

Fig. 10 Relation between ε^*_{3D} and Q/h_w^2 in multi-pass welding without external constraint.

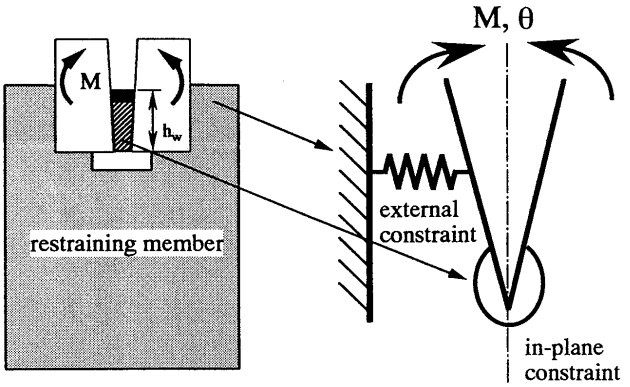

Fig. 11 Relation between constraints and ε^*_{3D}.

weld becomes 30 mm in this case. The difference between the two models observed in the early stage corresponds to the effect of moving heat source. Noting this fact, the inherent strain ε^* can be separated into the part determined by in-plane constraint ε^*_m and the part due to the effect of moving heat source ε^*_{3D}, such as,

$$\varepsilon^* = \varepsilon^*_m + \varepsilon^*_{3D} \tag{9}$$

Since the deformation can be assumed to be proportional to the heat input Q, ε^*_m is described in the following form.

$$\varepsilon^*_m = a_1 \frac{Q}{A} \tag{10}$$

Where, A is the cross-sectional area of the weld metal for the path under consideration and a_1 is an unknown constant. On the other hand, ε^*_{3D} representing the effect of moving heat source is plotted against the parameter Q/h_w^2 in **Fig. 10.** Noting that ε^*_{3D} is roughly proportional to Q/h_w^2, the following equation can be proposed.

$$\varepsilon^*_{3D} = \frac{Q}{a_2 h_w^2} \tag{11}$$

Figure 11 illustrates the physical meaning of the above equation. The effect of moving heat source is represented by moment M and it is proportional to Q. The resistance against this moment is the bending stiffness of the finished part of the weld with thickness h_W and it is proportional to $(h_w)^3$. Thus, the rotation angle θ becomes proportional to $Q/(h_w)^3$. Assuming that ε^*_{3D} is produced through the rotation θ, Eq. 11 is derived. By substituting Eqs. 10 and 11 into Eq. 9, the inherent strain for a plate without external constraint is given as,

$$\varepsilon^*(h_w) = a_1 \frac{Q}{A} + \frac{Q}{a_2 h_w^2} \tag{12}$$

The unknown constants a_1 and a_2 can be determined through fitting the curve to that for inherent strain directly estimated from the deformation computed by three-dimensional thermal-elastic-plastic analysis. **Figure 12** shows distributions of inherent strain estimated using Eq. 12 and direct estimation. Further, the deformation at the top of the groove is computed using the estimated inherent strain and compared with that computed by 3-D thermal-elastic plastic analysis in **Fig. 13.** The deformation due to the multi pass welding is estimated fairly well with the elastic analysis using the proposed inherent strain.

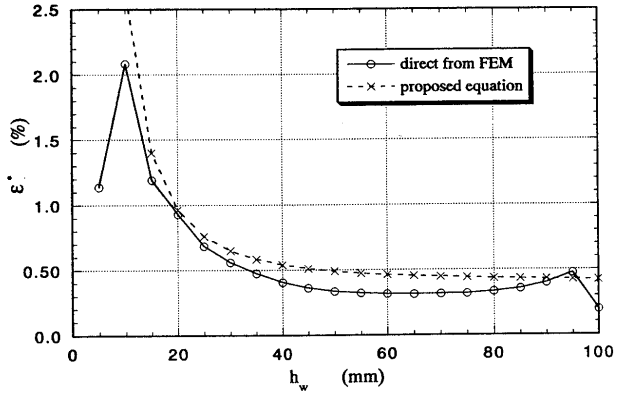

Fig. 12 Inherent strain estimated for model without external constraint using proposed equation.

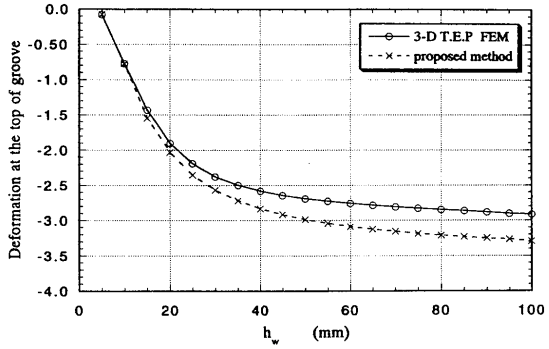

Fig. 13 Deformation at the top of groove predicted using proposed inherent strain (model without external constraint).

To study the phenomena in multi pass welding with external constraints, figures for Δδ/Δδ(1%) are drawn in the same manner as for the plate without external constraint. Figure 14 shows Δδ/Δδ(1%) curves for welding of thick plate with large external constraint shown in Fig. 2. Since, 3-D thermal-elastic-plastic FEM analysis is not performed due to extremely heavy computational load, experimental measurement is used. In **Fig. 14**, curves for the experiment and plane strain analysis are shown. The difference between these two curves observed up to h_W=150 mm is the effect of moving heat source. The effect of external constraint is slightly observed in the curve for plane strain analysis. To closely examine the effect of external constraint, the computed results for the models with small and large external constraint under plane strain condition are compared in **Fig. 15**. As it is seen from the figure, the effect of the external constraint on the inherent strain is relatively small but it extends more than 100 mm in terms of thickness of weld h_W.

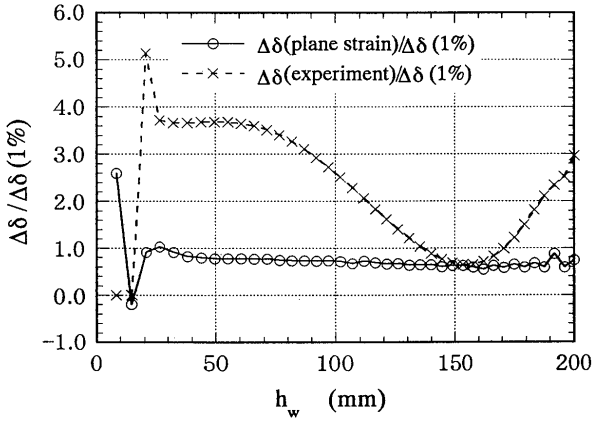

Fig. 14 Inherent strains estimated from experiment and plane strain analyses.

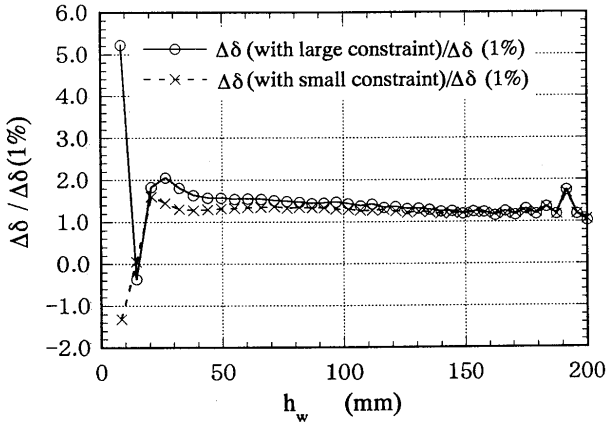

Fig. 15 Effect of external constraint on inherent strain.

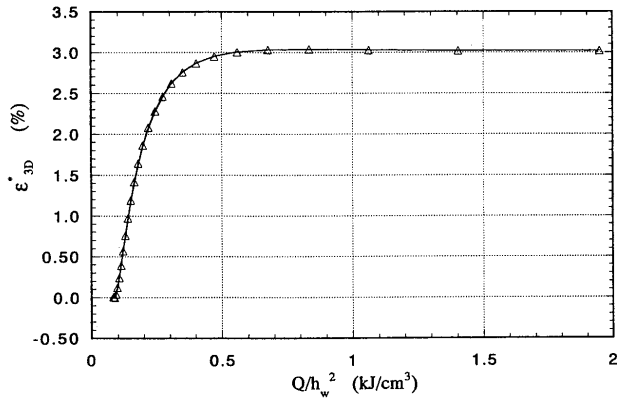

Fig. 16 Relation between ε^*_{3D} and Q/h_w^2 in multi-pass welding

The inherent strain ε^* for the multi pass welding with external constraint can be separated into ε^*_m and ε^*_{3D} as in the case of a plate without external constraint. Since, ε^*_m depends only on internal in-plane constraint and independent on external constraint, it can be described by Eq. 10. The effect of the external constraint need to be considered only in ε^*_{3D}. The component of inherent strain ε^*_{3D} estimated directly from the experiment conducted for the model with large constrain is plotted against Q/h_w^2 in **Fig. 16.** Unlike the case without external constraint, ε^*_{3D} is almost constant when Q/h_w^2 is large. This implies that in the early stage of multi-pass welding, the external constraint is dominant and the total constraint remains constant until in-plane constraint develops with number of paths. Considering the mechanical model described in Fig. 11, ε^*_{3D} can be described as,

$$\varepsilon^*_{3D} = \frac{a_3 Q}{K_{ex} + a_2 h_w^2} \tag{13}$$

Thus, the total inherent strain ε^* is given as,

$$\varepsilon^*(h_w) = a_1 \frac{Q}{A} + \frac{a_3 Q}{K_{ex} + a_2 h_w^2} \tag{14}$$

As seen from Fig. 2, the restraining members cover only half of the plate thickness. Considering this, the external constraint Kex is assumed in the following form,

$$K_{ex} = K_0\left(1 - \frac{h_w}{100}\right) \quad \text{if } 0 \le h_w \le 100 \tag{15}$$

$$K_{ex} = 0 \quad \text{if } 100 \le h_w \le 200$$

Unknown coefficients a_1, a_2, a_3 and K_0 involved in ε^* are determined by fitting curve to the measurement.

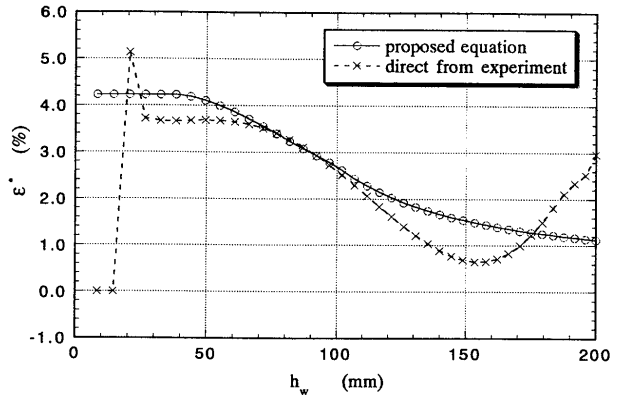

Fig. 17 Inherent strain estimated for model with external constraint using proposed equation.

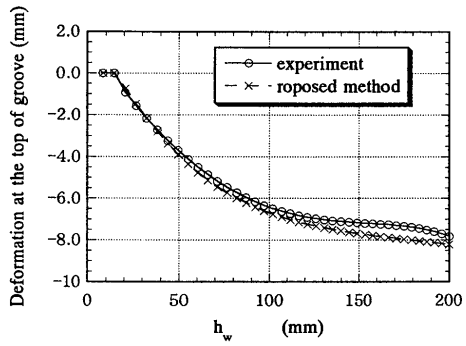

Fig. 18 Deformation at the top of groove predicted using proposed inherent strain (model with external constraint).

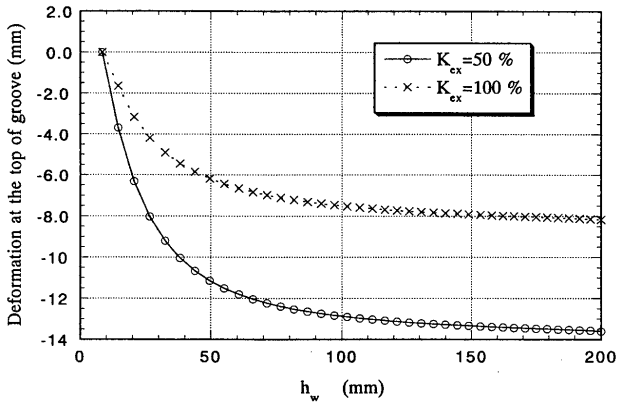

Fig. 19 Prediction of deformation at the top of groove for the model with external constraint of half strength.

The inherent strain estimated directly from the measurement and that using Eq. 14 are compared in **Fig. 17.** Also, the deformation at the top of the groove predicted by using inherent strain given by Eq. 14 is compared with the measurement. Good agreement is observed between them.

At present, only forms of the equations which determine the inherent strain ε^* as functions of the thickness of weld h_W are proposed. Further discussion on the values of constants is necessary. Once reliable database, which gives these constants, is established, deformation during the multi pass welding can be predicted through simple elastic FEM computation using the inherent strain. For example, the deformation when the external constraint is reduced to half can be easily predicted by the proposed method as shown in **Fig. 19.**

6. Conclusions

The characteristics of deformation at groove in multi-pass weld joint are clarified from the aspect of inherent strain. The inherent strain is governed by temperature and constraint. The constraint in multi-pass welding is separated into three parts, namely external constraint, in-plane constraint and effect of moving heat source. Taking this into account, equations to estimate the inherent strain are proposed for both welding joints with and without external constraint. The usefulness of the elastic FEM using the proposed inherent strain to predict the deformation at groove is demonstrated through numerical examples.

Acknowledgments

The authors would like to acknowledge that the data of the experiments cited in this report are provided by mitsubishi Electric Corporation.

References

1) M. Masubuchi, Trans. Soc. Naval Architects of Japan, 88(1955), 189-200 (in Japanese).
2) T. Fujimoto, J. Japan Welding Soc., 39-4, 236-252 (1970, in Japanese).
3) Y. Ueda, K. Fukuda and M. Tanigawa, Trans. ASME, J. Engineering Materials and Technology, 111, 1-8 (1989).
4) Y. Luo, H. Murakawa and Y. Ueda, Proc. 6-th International Symposium of JWS (Nagoya), 2, 551-556, (1996).